EEET ECOLOGICAL ENGINEERING & ENVIRONMENTAL TECHNOLOGY

Ecological Engineering & Environmental Technology, 2026, 27(3), 121–139
https://doi.org/10.12912/27197050/217987
ISSN 2719–7050, License CC-BY 4.0

Received: 2026.01.21
Accepted: 2026.02.20
Published: 2026.03.01

Seasonal plastic pollution risk in benthic ecosystems of the Bali Strait assessed using a pollution load index

I Putu Ranu Fajar Maharta[1,2*], I Gusti Bagus Sila Darma[1,2], I Wayan Arthana[1,2], Made Dharma Raharja[1], Made Narayana Adibhusana[1], I Gede Hendrawan[1,2]

[1] Department of Marine Science, Faculty of Marine and Fisheries, Udayana University (UNUD), Bukit Jimbaran, Badung, 80361 Bali, Indonesia
[2] Doctoral Program in Environmental Science, Universitas Udayana (UNUD), Denpasar City, 80232 Bali, Indonesia
* Corresponding author's e-mail: ranumaharta5@unud.ac.id

ABSTRACT

Plastic pollution poses a growing threat to benthic ecosystems in coastal waters, yet assessments often emphasize surface accumulation while overlooking seasonal variability and seafloor impacts. This study evaluates the spatial and seasonal variability of plastic pollution levels in benthic ecosystems of the Bali Strait, a monsoon influenced region characterized by intense human activities and ecologically valuable habitats. A hydrodynamic model coupled with Lagrangian particle tracking was used to simulate surface plastic transport under Southeast and Northwest Monsoon conditions and to identify potential accumulation zones based on residence time patterns. The Pollution Load Index was subsequently applied to quantify relative plastic pollution levels across benthic habitats, including coral reefs and seagrass meadows. Model validation against tidal elevations, surface currents, and drifter trajectories indicates satisfactory performance for seasonal circulation and transport analyses. Results reveal pronounced monsoon driven contrasts in plastic pollution levels on the seafloor. During the Southeast Monsoon, high to extreme pollution levels are concentrated along the western side of the Bali Strait, particularly in the Alas Purwo and Bama areas. In contrast, during the Northwest Monsoon, elevated pollution risk shifts toward the western and southern coasts of Bali, especially along Kuta Beach, while most locations along the East Java coast remain at low pollution levels. These patterns reflect the combined influence of seasonal current reversals, coastal orientation, and shoreline morphology on plastic retention and deposition. Overall, this study demonstrates that benthic plastic pollution in the Bali Strait is highly dynamic and seasonally controlled. Integrating hydrodynamic driven accumulation estimates with the pollution load index provides an operational framework for identifying seasonally vulnerable benthic habitats and supports adaptive monitoring and management strategies in monsoon-dominated coastal regions.

Keywords: residence time, pollution load index, benthic plastic pollution, monsoon variability, hydrodynamic modeling, Bali Strait, coastal ecosystems.

INTRODUCTION

Marine plastic debris is one of the most common types of pollution found in coastal and marine environments (Jambeck et al., 2015). Plastics have become the most dominant type of marine debris because of their low density, durability, and resistance to degradation, allowing them to persist for long periods and to be widely distributed following oceanographic dynamics (Bucknall, 2020; Derraik, 2002; UNEP, 2021). Over the last decade, increasing human activities on land and in coastal areas have driven the input of waste into marine ecosystems through river discharge, surface runoff, and coastal activities resulting from suboptimal waste management (Harding, 2016; Jambeck et al., 2015; Lau et al., 2020).

Studies on the distribution of plastic debris at the sea surface and in coastal areas have been widely conducted, both through direct observations

and modeling approaches (Lambert et al., 2020; Lebreton et al., 2018; Rothäusler et al., 2019). At the sea surface, studies generally show that the main drivers of floating plastic distribution are controlled by current dynamics, wind, and coastal morphology, which can form seasonal accumulation patterns (Lebreton et al., 2018; Maximenko et al., 2012; van Sebille et al., 2015). In tropical regions such as Indonesia, which e xperience strong seasonal variability associated with monsoon systems, the direction and intensity of winds and surface circulation are strongly affected and play an important role in redistributing plastic debris between seasons (Napper et al., 2021; Wang et al., 2021; Yin et al., 2023). The influence of monsoon conditions on riverine plastic discharge is particularly significant because rainfall is very high during the northwest monsoon (December, January, and February), leading to increased plastic inputs from land to the ocean, whereas rainfall becomes lower during the southeast monsoon (June, July, and August), resulting in reduced plastic discharge (Cordova et al., 2022). In addition, coastal areas with high human activity, such as tourism zones and waters supporting major coastal ecosystems, exhibit high vulnerability to plastic pollution exposure (Auta et al., 2017; Thushari and Senevirathna, 2020). The Bali Strait in Indonesia represents an example of a coastal region with high ecological value, as it serves as a center of tourism activity while supporting benthic ecosystems such as coral reefs and seagrass meadows that are sensitive to pollution pressure (Boakes et al., 2022; Intyas et al., 2025; Maharta et al., 2020, 2021; Suteja et al., 2021). Specifically in the Bali Strait, the distribution of marine debris at the sea surface and the spatial patterns of stranded debris along the coastline are strongly influenced by monsoon variability (Maharta et al., 2021; Suteja et al., 2021).

Although marine plastic pollution has been extensively studied, most research has focused on the distribution and accumulation of plastics at the sea surface and in coastal areas (Lebreton et al., 2018; Maximenko et al., 2012; van Sebille et al., 2015). This approach has limitations in explaining the ultimate fate of plastics in the marine environment, particularly the transfer processes from the surface to the water column and the seafloor. The mismatch between estimates of plastic inputs to the ocean and the volume of plastics observed at the surface suggests that a large proportion of plastics is likely stored in less-observed marine compartments, especially benthic environments (Cózar et al., 2015; Kooi et al., 2017). On the other hand, these studies are generally sporadic and spatially limited, and therefore have not yet been able to comprehensively describe patterns of benthic plastic accumulation (Bergmann et al., 2017).

The linkage between oceanographic dynamics and the potential accumulation of plastics on the seafloor has rarely been analyzed explicitly, making research outcomes difficult to transform into an integrated and operational pollution risk assessment framework. However, this limitation can be addressed through approaches that link physical water dynamics with the potential transfer of plastics to benthic environments. In oceanography, residence time is used to represent the degree of retention of water masses and materials within a given water body (Brauwere et al., 2011; Clayer et al., 2024; Paul et al., 2017; Rosas et al., 2022). Areas with high residence time, such as regions with low current velocities, eddies, and semi-enclosed coastlines, can enhance the interaction of plastics with vertical processes, allowing this parameter to be used as an indirect indicator for estimating the potential accumulation of sinking plastics (Brauwere et al., 2011; Politikos et al., 2020; Wu et al., 2022; Zhou et al., 2020). This approach is practical because it can be applied using outputs from hydrodynamic models and particle tracking simulations (Critchell and Lambrechts, 2016; Liubartseva et al., 2018). Locally, the Bali Strait contains several coastal areas characterized by low current velocities in its wider sections, concave shoreline configurations such as those along the coast of Badung Regency, and the presence of small eddies in the central part of the strait (Adibhusana et al., 2023; Maharta et al., 2021).

However, estimating the potential for sinking plastics alone is not sufficient to assess their pollution implications for seafloor ecosystems, because the Bali Strait contains benthic ecosystems that function as key ecological, economic, and tourism supports. Therefore, the pollution load index (PLI), which has been widely used as a quantitative indicator of environmental pollution levels (Patterson et al., 2022b; Praved et al., 2025; Zheng et al., 2023), can be adapted to evaluate the level of plastic pollution in benthic ecosystems. Based on this framework, this study aims to assess the spatial and seasonal levels of plastic pollution in benthic ecosystems of the Bali Strait. This assessment is conducted by

integrating estimates of sinking plastic distribution based on hydrodynamic processes with the PLI as a pollution indicator, to support understanding of plastic pollution risks in ecologically valuable and anthropogenically pressured coastal regions.

MATERIALS AND METHODS

Research location and model design

This study was conducted in the waters of the Bali Strait, which separates Java Island and Bali Island (Figure 1). To estimate plastic pollution risk in benthic ecosystems, several methodological steps were applied, beginning with the simulation of ocean current dynamics used as input for river-based plastic tracking models (Figure 2). The first step involved hydrodynamic model simulations using the Finite volume community ocean model (FVCOM) to characterize surface current patterns, driven by meteorological and oceanographic forcing data (Figure 2A). The second step consisted of plastic particle tracking simulations using two scenarios: Scenario 1 (Figure 2B1) was designed to calculate surface plastic residence time, while Scenario 2 (Figure 2B2) was applied to simulate river-derived plastic transport to estimate surface plastic density. The third step involved spatial overlay analysis of residence time (Figure 2B1), surface plastic density (Figure 2B2), and benthic ecosystem locations to estimate the potential accumulation of plastics in benthic ecosystems. Based on this integration, the levels of plastic pollution in benthic ecosystems of the Bali Strait were quantified (Figure 3C). Model simulations in this study were conducted for both the rainy season (Northwest Monsoon) and the dry season (Southeast Monsoon).

Hydrodynamic model

The hydrodynamic model in this study was simulated using finite volume community ocean model (FVCOM) version 4.3 (www.fvcom.org) to solve the continuity and momentum equations (Equations 1–3), as well as the temperature (Equation 4), salinity (Equation 5), and density equations (Equation 6) (Chen et al., 2013). The model coefficients include vertical eddy viscosity and thermal diffusion coefficients, which are calculated using the modified Mellor–Yamada level 2.5 (MY-2.5) turbulence closure scheme (Galperin et al., 1988), then, horizontal diffusion coefficients are parameterized using the Smagorinsky eddy parameterization method (Chen et al., 2013). The model was implemented over a domain covering the Bali Strait and surrounding waters (Figure 2)

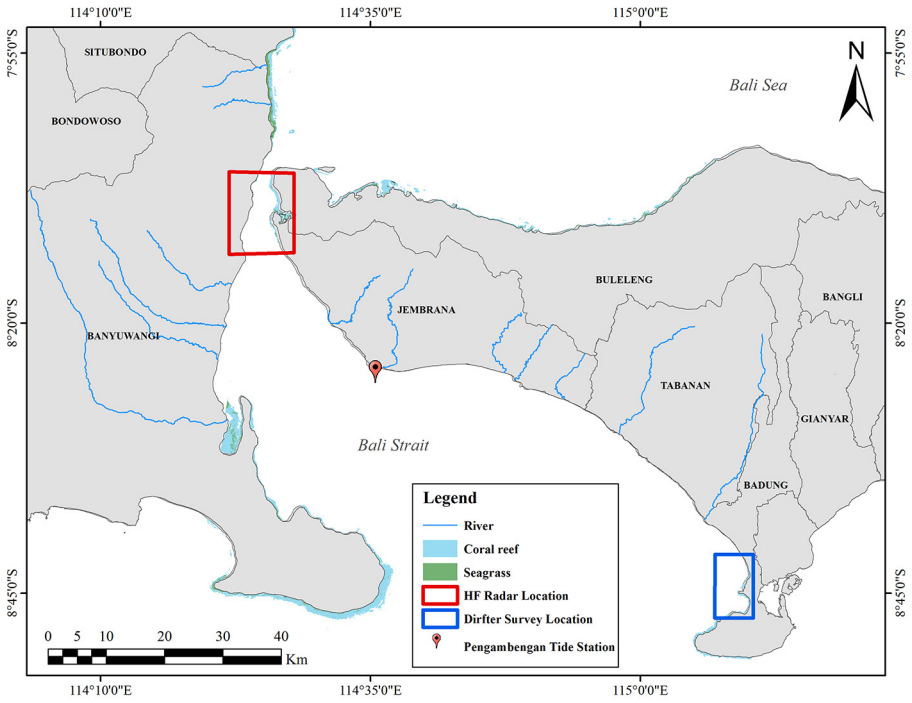

Figure 1. Study area showing benthic ecosystem (coral reef and seagrass) and validation locations

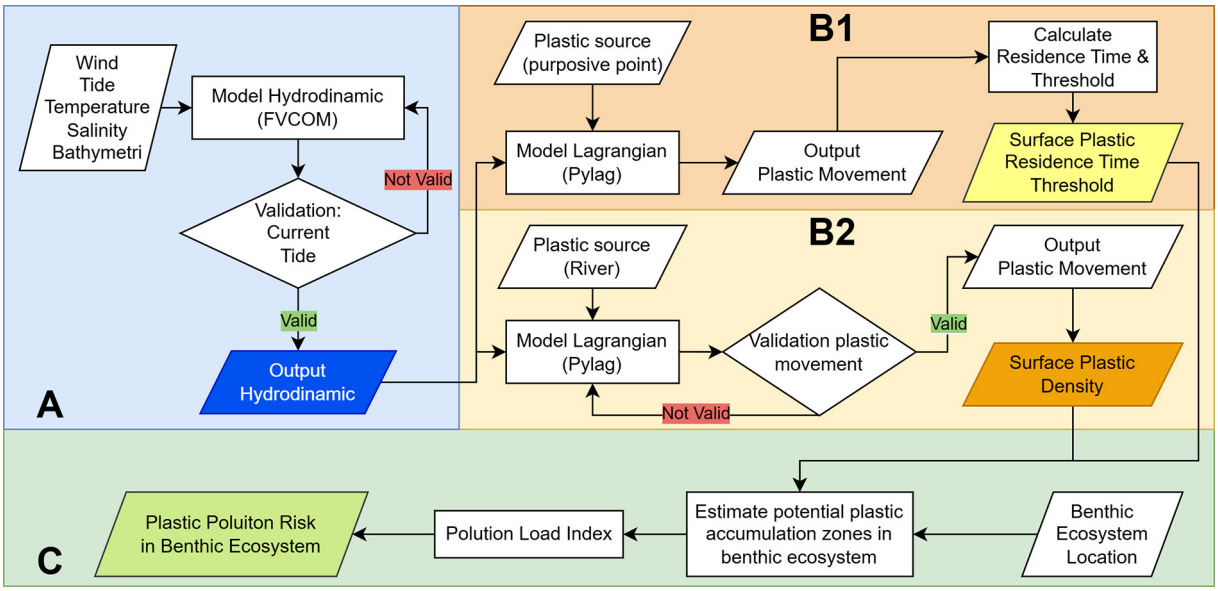

Figure 2. Model design flowchart illustrating (A) the hydrodynamic model, (B) the plastic tracking model, (C) plastic pollution risk in benthic ecosystems.

$$\frac{\partial \zeta}{\partial t}+\frac{\partial Du}{\partial x}+\frac{\partial Dv}{\partial y}+\frac{\partial \omega}{\partial \sigma}=0 \tag{1}$$

$$\begin{aligned}&\frac{\partial uD}{\partial t}+\frac{\partial u^2D}{\partial x}+\frac{\partial uvD}{\partial y}+\frac{\partial u\omega}{\partial \sigma}-fvD\\&=-gD\frac{\partial \zeta}{\partial x}-\frac{gD}{\rho_0}\left[\frac{\partial}{\partial x}\left(D\int_\sigma^0 \rho d\sigma'\right)+\sigma\rho\frac{\partial D}{\partial x}\right]+\\&+\frac{1}{D}\frac{\partial}{\partial \sigma}\left(K_m\frac{\partial u}{\partial \sigma}\right)+DF_x\end{aligned} \tag{2}$$

$$\begin{aligned}&\frac{\partial vD}{\partial t}+\frac{\partial v^2D}{\partial x}+\frac{\partial uvD}{\partial y}+\frac{\partial v\omega}{\partial \sigma}-fuD\\&=-gD\frac{\partial \zeta}{\partial y}-\frac{gD}{\rho_0}\left[\frac{\partial}{\partial y}\left(D\int_\sigma^0 \rho d\sigma'\right)+\sigma\rho\frac{\partial D}{\partial y}\right]+\\&+\frac{1}{D}\frac{\partial}{\partial \sigma}\left(K_m\frac{\partial u}{\partial \sigma}\right)+DF_y\end{aligned} \tag{3}$$

$$\begin{aligned}&\frac{\partial TD}{\partial t}+\frac{\partial T\,uD}{\partial x}+v\frac{\partial TvD}{\partial y}+\frac{\partial T\omega}{\partial \sigma}=\\&=\frac{1}{D}\frac{\partial}{\partial \sigma}\left(K_h\frac{\partial T}{\partial \sigma}\right)+D\hat{H}+DF_t\end{aligned} \tag{4}$$

$$\begin{aligned}&\frac{\partial SD}{\partial t}+\frac{\partial SuD}{\partial x}+v\frac{\partial SvD}{\partial y}+\frac{\partial S\omega}{\partial \sigma}=\\&=\frac{1}{D}\frac{\partial}{\partial \sigma}\left(K_h\frac{\partial S}{\partial \sigma}\right)+DF_s\end{aligned} \tag{5}$$

$$\rho=\rho(T,S) \tag{6}$$

where: x, y, and σ are directions for east and west, north and south, and also vertical in the Cartesian coordinate system; u, v, and ω are the components of the current velocity for the x, y, and σ directions; T is the temperature (°C); S is salinity (PSU); ρ is the density (kg/m^3) while ρ_0 is the initial density (kg/m^3); f is the Coriolis force (°); g is gravity (m/s^2); K_m is the vertical eddy viscosity (m^2/s); and K_h is the thermal vertical eddy diffusion coefficient (m^2/s). F_x, F_y, F_t, and F_s represent friction in the x and y directions, thermal, and salinity diffusion (N); D is the total depth of the water column (m); ζ is the height of the water surface elevation (m).

The hydrodynamic model using an unstructured grid with spatial resolutions ranging from 100 m to 5 km (Figure 3) and applied 20 sigma-coordinate vertical layers. The primary input for the model included bathymetric data obtained from the National Bathymetry Dataset of Indonesia, managed by Geospatial Information Agency (BIG) (Figure 3). At the open boundaries, tidal elevation data were prescribed using the tide model driver (TMD). Temperature and salinity at the open boundaries were specified based on outputs from the HYbrid Coordinate Ocean Model (HYCOM). In addition, surface meteorological forcing was applied using data from ECMWF Reanalysis Version 5 (ERA5), as summarized in Table 1.

Validation of the hydrodynamic model results was performed using observed surface current data from the high frequency (HF) Radar system provided by Indonesian Meteorological and Climatological Agency (BMKG) in

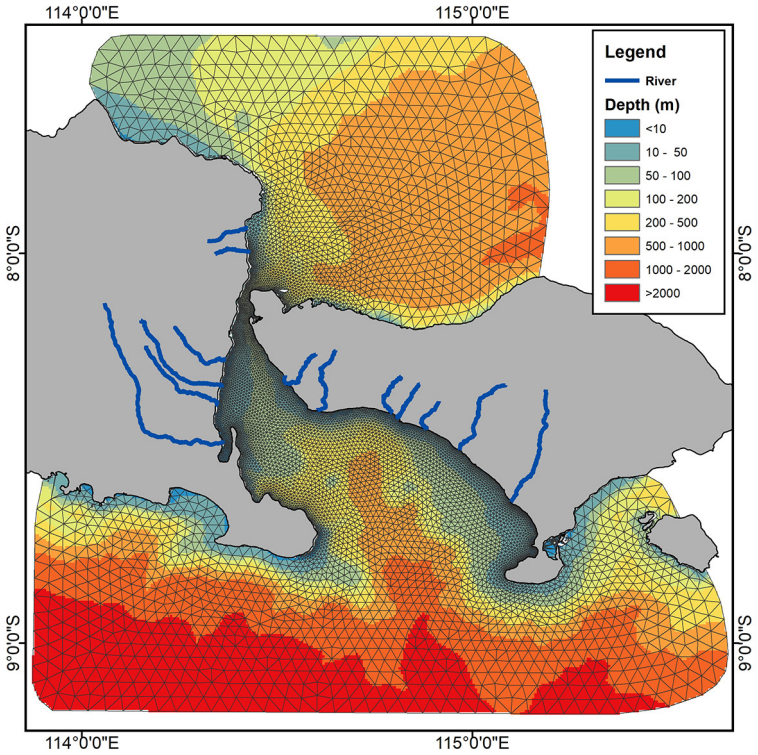

Figure 3. Model grid and bathymetry

the Bali Strait, along with tidal elevation observations supplied by BIG at Pengambengan tide station (Figure 1).

Plastic tracking model

The plastic tracking model in this study was simulated using Python Lagrangian (PyLag) version 06 (https://pylag.readthedocs.io/en/latest), which is an offline particle tracking model fully integrated with FVCOM. In this study, the Lagrangian method implemented in PyLag was applied to solve the differential equation describing particle motion in the water (Equation 7) (Uncles et al., 2020). This equation provides a mathematical representation of particle movement under the hydrodynamic conditions of the study area.

$$\rho = \rho(T, S) \tag{7}$$

where: $r_i = X_i\,(t = t_0)$ the position vector of particle i at the initial time t = t_0, and U_i epresents the particle velocity vector. For passive transport, the particle velocity is assumed to be equal to the fluid velocity at the particle location, such that $U_i = [u(t,x)]\ x = {}_{xi}$, where u is the fluid velocity vector obtained from the hydrodynamic model output.

The particle velocity vector is subsequently decomposed into resolved and unresolved components to account for subgrid-scale processes that are not explicitly resolved by the hydrodynamic model. These components are then incorporated into a random displacement model (Equation 8).

$$dX_j = \left[u_j + \frac{\partial D_{jk}}{\partial x_k}\right] dt + \\ + \left(2D_{jk}\right)^{\frac{1}{2}} dW_k \tag{8}$$

where: $dH_j = dX$ represents the incremental change in particle position, D_{jk} is the diffusion tensor, and dW_k represents an incremental Wiener process that introduces stochastic behavior into the particle trajectory simulations.

To ensure a realistic representation of the spatial distribution of plastic litter in the Bali Strait, plastic release configurations were designed under two different scenarios according to the objectives of the analysis (Figure 4). The first scenario (Figure 2B1) applied a uniform plastic release across the entire Bali Strait domain (purposive point). In this scenario, plastics were released at the sea surface on a regular grid with an inter-particle spacing of approximately 1 km (Figure 4).

Table 1. Hydrodynamic model design

Parameters	Information	
Grid	Unstructured triangular grid with resolution 200 m – 5 km (Distance Between the 2 Closest Nodes).	
Layer	20 sigma layers.	
Bathymetry	National Bathymetry Dataset of Indonesia – Geospatial Information Agency Indonesia: (https://sibatnas.big.go.id/).	
Time step (external mode)	1 second	
Time step (internal mode)	10 seconds	
Time simulation	SE Monsoon: 1 June - 31 August 2024	
	NE Monsoon: 1 December 2023 – 28 February 2024	
Open boundary	Tide elevation	TMD: (https://www.mathworks.com/matlabcentral/fileexchange/133417-tide-model-driver-tmd-version-3-0).
	• Temperature • Salinity	HYCOM: (https://www.hycom.org/).
Meteorological condition	• Wind • Air pressure • Heat flux • Precipitation • Evaporation	ERA – 5: (https://cds.climate.copernicus.eu/datasets/reanalysis-era5-single-levels?tab=overview).
Validation data	Current observation data (1 December 2023 – 28 February 2024 & 1 June - 31 August 2024)	HF Radar: (https://maritim.bmkg.go.id/radar)
	Tide observation data (1 December 2023 – 28 February 2024 & 1 June - 31 August 2024)	BIG tide station data: (https://srgi.big.go.id/tides)

This configuration was intended to calculate location based residence time, defined as the duration plastics remain within a given area in response to surface current dynamics and dispersive processes. By applying a homogeneous release over the entire domain, the resulting residence time map reflects hydrodynamic retention characteristics controlled by the geometry of the Bali Strait and seasonal current variability, independent of specific source locations.

The second scenario (Figure 2B2) focused on plastic release from river mouths as representations of land based plastic sources, with subsequent plastic transport simulated using PyLag and validated against drifter observations collected near the coastal waters of Badung Regency (Figure 1). The release locations and the number of plastics discharged from each river were determined based on the PISCES dataset (https://www.piscespartnership.org/) (Figure 4), ensuring consistency with the available river mouth inventory. The number of plastics released from each river was adjusted according to the PISCES dataset to represent differences in relative source contributions. Plastic release was conducted continuously at 6-hour intervals to capture variability in riverine plastic input interacting with tidal dynamics and sub-daily current variability.

Validation of the plastic tracking model was performed by comparing simulated plastic trajectories with observational data. Observations of plastic movement were obtained from a Davis drifter experiment conducted on 3 February 2019 for approximately 6 hours, representing one tidal cycle. The drifter deployment location was selected in an offshore area to minimize the influence of longshore currents and coastal boundary effects (Figure 1). Although the plastic tracking simulations were carried out using the 2024 hydrodynamic configuration, the 2019 drifter observations were used for validation due to data availability constraints, under the assumption that the dominant seasonal circulation characteristics in the Bali Strait remain relatively consistent between years.

Calculation of potential plastic accumulation zones in benthic ecosystems

To quantify the potential plastic accumulation zones in benthic ecosystems, indicators derived from the plastic tracking model were subsequently integrated into a pollution load index (PLI) framework. Three primary variables were considered surface residence time, surface plastic density, and the location of benthic ecosystems.

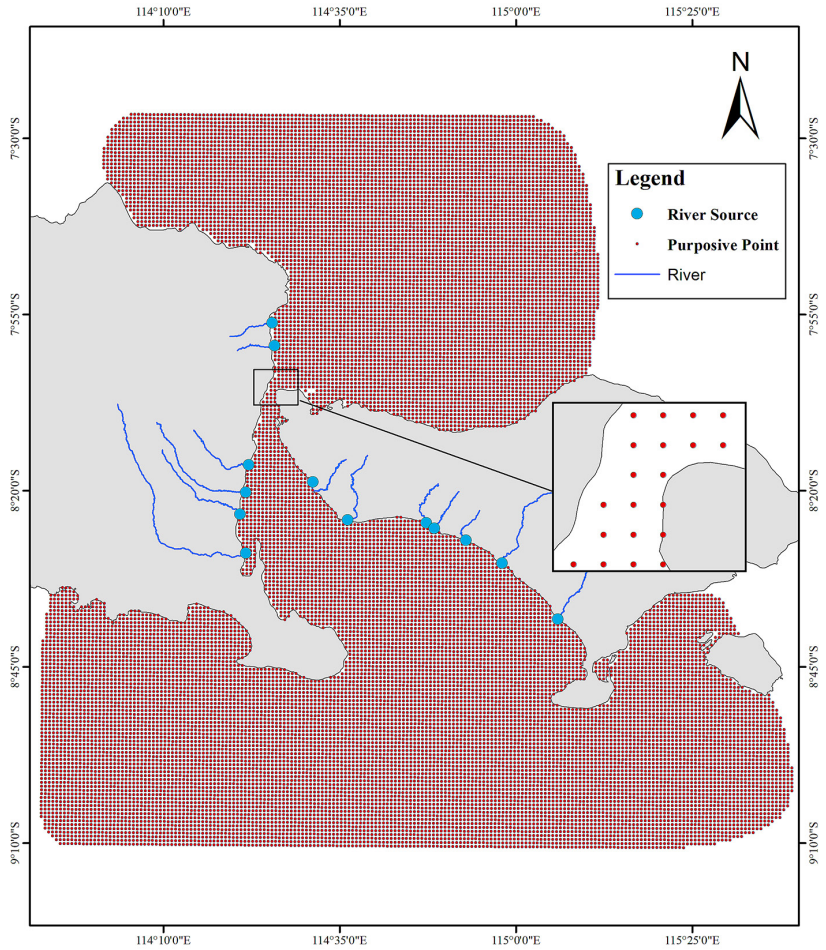

Figure 4. Plastic source location (red points for scenario 1 and blue points for scenario 2)

Residence time was used as the primary parameter to identify marine areas with potential plastic accumulation at the sea surface. In the context, residence time is defined as the duration a plastic remains within a given area before being exported by advective processes (Brauwere et al., 2011; Clayer et al., 2024; Paul et al., 2017; Rosas et al., 2022). This parameter has been widely applied to characterize retention zones, weakly flushed areas, and regions with limited horizontal transport in coastal waters and narrow straits.

Residence time was calculated based on plastic trajectories generated from the plastic tracking model (Figure 2 B1) under the uniformly distributed plastic release scenario across the entire model domain (Figure 4). For each plastic *i*, residence time was defined as the time interval between the moment the plastic entered the analysis area and the moment it exited the area (Equation 9).

$$RT_i = t_{\text{exit},i} - t_{\text{entry},i} \tag{9}$$

where: RT_i is the residence time of the *i*, plastic $t_{entry,i}$ is the time when the plastic enters the analysis area, and $t_{exit,i}$ is the time when the plastic leaves the area. Spatial residence time values were then obtained by calculating the mean residence time of all plastics passing through each grid cell within the model domain.

The resulting spatial distribution of residence time represents the retention characteristics of surface waters controlled by current dynamics, independent of the spatial distribution of land-based plastic sources. Areas characterized by high residence time indicate relatively weak horizontal circulation and low plastic export efficiency, thereby providing favorable conditions for plastic retention (Critchell et al., 2015; Critchell and Lambrechts, 2016; van Sebille et al., 2015).

To objectively delineate high retention zones, a percentile-based threshold was applied to the spatial residence time distribution. High residence-time zones were defined as grid cells with residence time values exceeding the 90th percentile of the residence time distribution across

the model domain $P_{90}(RT)$. The residence time threshold (RT_{thr}) (Equation 10).

$$RT_{\text{thr}} = P_{90}(RT) \tag{10}$$

A grid cell j was classified as a high-retention zone (Equation 11).

$$RT_j \geq RT_{\text{thr}} \tag{11}$$

This percentile-based approach allows the identification of relative retention hotspots that emerge directly from the modeled hydrodynamic conditions, rather than relying on a prescribed absolute time threshold. As such, it provides a robust and transferable method for detecting areas with reduced horizontal transport and enhanced potential for plastic retention under varying hydrodynamic regimes.

Surface plastic density (D_p) was expressed as the mean number of plastic particles per unit area (pcs km^{-2}) and derived from the plastic tracking results of Scenario 1 (Figure 2B2) by calculating the average spatial concentration of plastics at the sea surface over the simulation period. For each grid cell j (Equation 12).

$$D_{p,j} = \frac{1}{T}\sum_{t=1}^{T}\frac{N_j(t)}{A_j} \tag{12}$$

where: $D_{p,j}$ is the mean surface plastic density in grid cell j (pcs km^{-2}), $N_j(t)$ is the number of plastic particles present in grid cell j at time step t, A_j is the area of grid cell j (km^2), and T is the total number of time steps considered in the analysis. This averaging approach provides a temporally integrated representation of surface plastic distribution, reducing the influence of short-term variability and highlighting persistent plastic hotspots across the study area.

The third variable consisted of benthic ecosystem maps represented as polygon features (Figure 1), which define the spatial extent of distinct benthic habitats (coral reef and seagrass). In addition, benthic ecosystem maps were obtained from the Allen Coral Atlas (https://allencoralatlas.org/) and were used for spatial overlay analyses between potential plastic accumulation zones and benthic ecosystems. These polygons were used as spatial units for pollution assessment. A spatial overlay analysis was performed by intersecting (1) the high-retention residence time zones, (2) surface plastic density fields, and (3) benthic ecosystem polygons. For each benthic ecosystem polygon, surface plastic density values located within high retention zones were extracted and spatially aggregated.

Pollution load index (PLI) assessment

The level of plastic pollution on the seabed was evaluated using the PLI to represent relative pollution pressure at each spatial unit (Patterson et al., 2022a; Tomlinson et al., 1980). In this study, the PLI input was derived from the amount of plastic entering potential plastic accumulation zones overlaid with underwater habitat maps.

The plastic density value at each grid cell ($x'y$), expressed as $C_i(x, y)$, was calculated from the weekly amount of plastic entering the plastic accumulation zones in benthic ecosystems during one seasonal simulation period (three months) (Equation 13).

$$C_i(x,y) = \frac{1}{12}\sum_{k=1}^{12} D_{p,j}\,(x,y) \tag{13}$$

where: $D_{p,j}(x, y)$ represents the number of sinking plastic particles from mean surface plastic density during the k-th week in grid cell (x, y). The background concentration value C_{0i} was defined as the minimum number of sinking plastics identified across the entire study domain by considering both simulation seasons (northwest monsoon and southeast monsoon) (Equation 14).

$$C_{0i}(x,y) = \min\begin{pmatrix} D_{p,j,\text{min,west}}(x,y), \\ D_{p,j,\text{min,east}}(x,y) \end{pmatrix} \tag{14}$$

The contamination factor for each grid cell was calculated in Equation 15.

$$CF_i(x,y) = \frac{C_i(x,y)}{C_{0i}(x,y)} \tag{15}$$

Subsequently, the PLI value for each grid cell was determined based on the contamination factor as Equation 16.

$$PLI_i(x,y) = \sqrt{CF_i(x,y)} \tag{16}$$

The PLI values were then spatially mapped onto benthic habitat units derived from the overlay of underwater habitat maps and plastic accumulation distributions. This spatial distribution

of PLI was used to evaluate the relative level of plastic pollution in benthic ecosystems. Interpretation of PLI values followed the hazard classification as follows: PLI < 10 (minor), 10 ≤ PLI < 20 (moderate), 20 ≤ PLI < 30 (high), and PLI ≥ 30 (extreme danger).

Model validation

The model validation employed statistical indicators commonly used in oceanographic modeling studies, namely the root mean square error (RMSE), Pearson correlation coefficient (r), and Willmott's index of agreement (d).

RMSE was used to quantify the absolute error between model results and observations (Chai and Draxler, 2014; Willmott and Matsuura, 2005) (Equation 17).

$$\mathrm{RMSE} = \sqrt{\frac{1}{n}\sum_{i=1}^{n}(M_i - O_i)^2} \qquad (17)$$

where: M_i and O_i represent the modeled and observed values, respectively, and $n$denotes the number of data points.

The Pearson correlation coefficient (r) was applied to assess the strength of the linear relationship between modeled and observed values (Pearson, 1895) (Equation 18).

$$r = \frac{\sum(M_i - \bar{M})(O_i - \bar{O})}{\sqrt{\sum(M_i - \bar{M})^2 \sum(O_i - \bar{O})^2}} \qquad (18)$$

where: $\bar{M}$ and $\bar{O}$ denote the mean values of the modeled and observed datasets, respectively.

The strength of the linear relationship was interpreted based on the absolute value of the Pearson correlation coefficient. Values of $|r| < 0.20$ indicate a very weak or negligible linear relationship, values between 0.20 and 0.39 indicate a weak relationship, values between 0.40 and 0.59 represent a moderate relationship, values between 0.60 and 0.79 indicate a strong relationship, and values of $|r| \geq 0.80$ indicate a very strong or near-perfect linear relationship. This classification was used to evaluate the level of agreement between modeled and observed data during the model validation process.

In addition, Willmott's Index of Agreement (d) was used to evaluate the overall degree of agreement between model predictions and observations (Willmott et al., 2012) (Equation 19).

$$d = 1 - \frac{\sum(M_i - O_i)^2}{\sum(|\, M_i - \bar{O}\,| + |\, O_i - \bar{O}\,|)^2} \qquad (19)$$

This combination of statistical metrics provides a comprehensive assessment of model accuracy, linear association, and overall agreement between simulated and observed data. Model validation was conducted to evaluate the performance of the hydrodynamic and plastic tracking simulations by comparing model outputs with observational data. For the hydrodynamic model, tidal elevation data were validated using the RMSE and the Pearson correlation coefficient, and the differences between modeled and observed tidal levels were also quantified. In addition, surface current velocities were validated using HF Radar observations, where the Pearson correlation coefficient was applied to assess the similarity of current patterns, and Willmott's Index of Agreement was used to evaluate the overall degree of agreement between model predictions and observations. Plastic tracking simulations were validated using drifter observations by comparing modeled particle trajectories with observed drifter movements. The validation focused on assessing whether the modeled plastic transport exhibited movement patterns consistent with the trajectories observed in the field.

RESULTS

Model performance and validation

Model performance was evaluated through validation of surface currents (u and v components), tidal elevations, and plastic movement by comparing simulation results with available observational data. The validation was conducted for two seasonal periods, namely the northwest monsoon and the southeast monsoon, with simulation periods adjusted to match the observational data intervals.

The tidal elevation validation results indicate a good level of agreement between the model and observations for both seasons (Figure 5). During the northwest monsoon, the correlation coefficient reached 0.91 with an RMSE of 0.27 m,

while during the southeast monsoon the correlation coefficient was 0.89 with an RMSE of 0.29 m. The modeled tidal amplitude and phase generally show strong consistency with the observational data (Figure 5).

Validation of surface currents indicates differences in model performance between current components. During the northwest monsoon, the u (east–west) current component exhibits relatively low to moderate correlation values (0.04–0.60), whereas the v (north–south) component shows higher correlations, exceeding 0.7 at most locations. Willmott's index of agreement values are also higher for the v component than for the u component, indicating better model performance in representing the dominant current direction (Figure 6a). A similar pattern is observed during the southeast monsoon, with v component correlations ranging from 0.5 to 0.8, while the u component generally exhibits lower correlations (Figure 6b).

Validation of plastic tracking shows that the modeled plastic trajectories can represent the general patterns of observed drifter trajectories, although positional differences occur at certain times (Figure 7). Overall, the validation results indicate that the model performance is sufficient for application in surface transport analysis, residence time calculations, and identification of potential plastic accumulation zones in subsequent analyses.

Surface circulation

The surface current circulation patterns in the Bali Strait, derived from the hydrodynamic model simulations, exhibit a strong influence of strait geometry and seasonal monsoonal wind variability. In the narrow sections of the strait, residual currents during both seasons consistently flow southward, reflecting the transport of water masses toward the Indian Ocean because of the constricted strait topography (Figure 8).

In the more open waters south of Bali, surface current patterns exhibit clear seasonal variability. During the northwest monsoon, the dominant currents flow east-southeastward under the influence of the Northwest Monsoon winds, whereas during the southeast monsoon the dominant currents shift northwestward in response to the Southeast Monsoon winds (Figure 8). The highest current velocities are identified in the northwest section of the Bali Strait, ranging from approximately 0.35 to 0.45 m/s, while lower velocities (0.1–0.25 m/s) are observed in the more open waters to the north and south of the strait. This pattern is consistent with the characteristics of regional circulation in Indonesian waters, which are influenced by the interaction between strait throughflow and monsoonal winds.

Spatial distribution of residence time and potential plastic accumulation zones

The spatial distribution of surface residence time and potential plastic accumulation zones presented in this section was derived from the plastic tracking model simulations. Specifically, Scenario 1 was designed to generate surface residence time fields, while Scenario 2 was used to estimate surface plastic density originating from riverine sources.

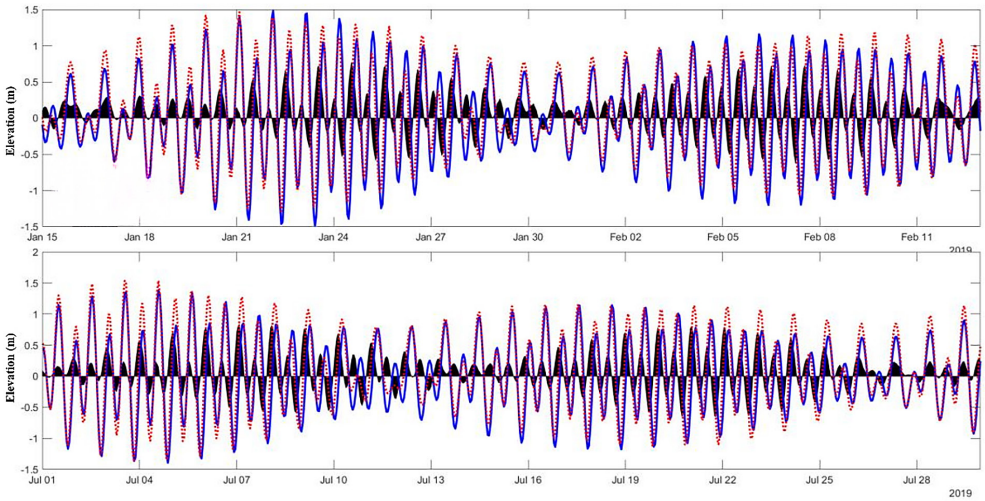

Figure 5. Validation of tidal elevations for the northwest (top) and southeast (bottom) monsoon. Black area is difference, blue line is observation data, red dashed line is model data

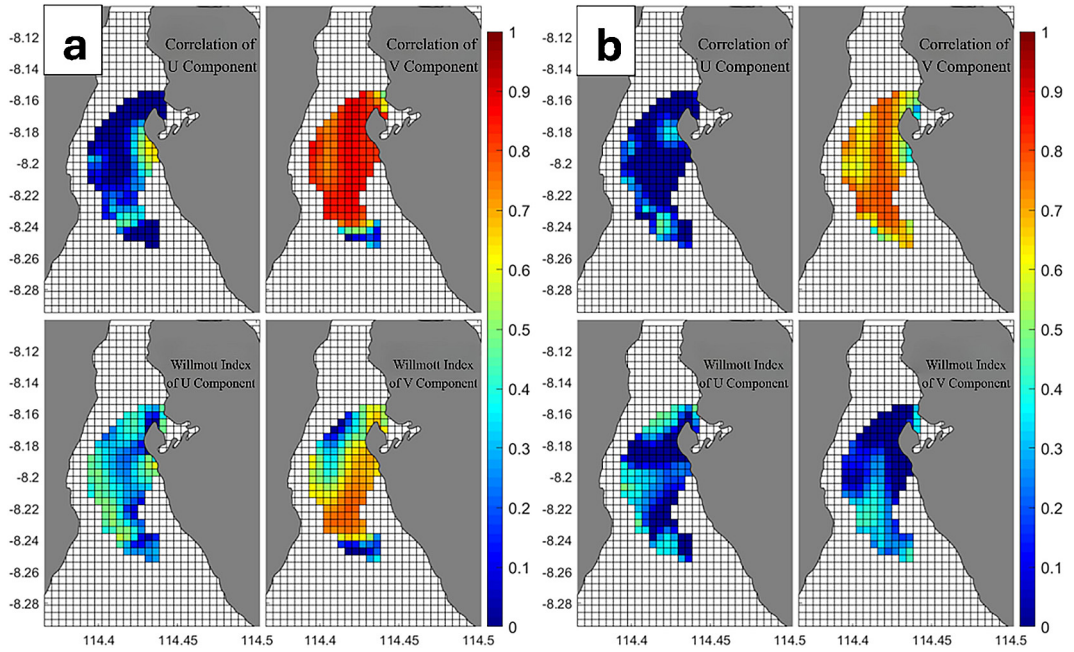

Figure 6. Correlation (top) and Willmott index (bottom) between component u (left) and component v (right) of model data and observations. (a) northwest monsoon and (b) southeast monsoon

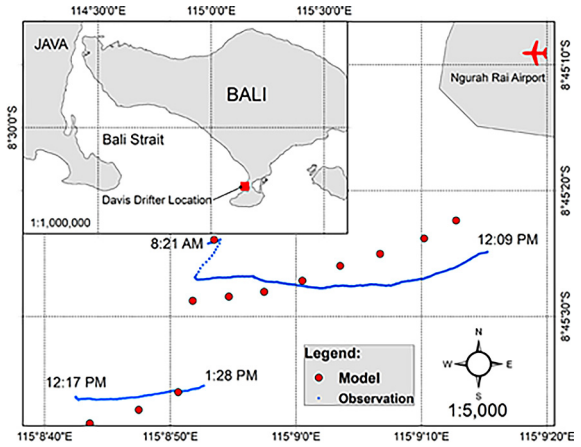

Figure 7. Validation of plastic tracking by comparison between modeled particle trajectories (red points) and observed davis drifter trajectories (blue points)

The modeling results indicate that residence time values in the Bali Strait (Figure 9) derived from Scenario 1. Mean residence time during the northwest monsoon is higher (17.8 ± 2.4 hours) than during the southeast monsoon (8.6 ± 2.1 hours), indicating stronger particle retention in the northwest monsoon. During the northwest monsoon, high residence time zones (≥ 15 hours) are mainly distributed along the eastern side of the Bali Strait, including the western coast of Bali Island (e.g., Badung and Jembrana) and several semi-enclosed waters, with maximum values reaching up to 92 hours along the Badung coast. In contrast, low residence time values (< 6 hours) dominate the more open western part of the strait, particularly along the northern coast of Banyuwangi. During the southeast monsoon, zones of elevated residence time shift toward the western side of the Bali Strait, especially along the eastern coast of Banyuwangi in Java and Gilimanuk Bay in Jembrana, Bali, where maximum values reach approximately 44 hours, while several areas along the western coast of Bali continue to exhibit locally high retention due to coastal geometry and localized circulation patterns.

Following the residence time-based methodology described earlier, high retention zones were objectively identified using a percentile-based threshold. In this study, grid cells exceeding the 90th percentile of the residence time distribution were classified as high retention zones. The calculated value of this threshold corresponds to a residence time of approximately 6 hours, which therefore represents the minimum residence time associated with enhanced retention conditions in the Bali Strait. These high retention zones are subsequently interpreted as potential plastic accumulation zones, as reduced horizontal transport in these areas increases the likelihood of prolonged plastic residence and accumulation.

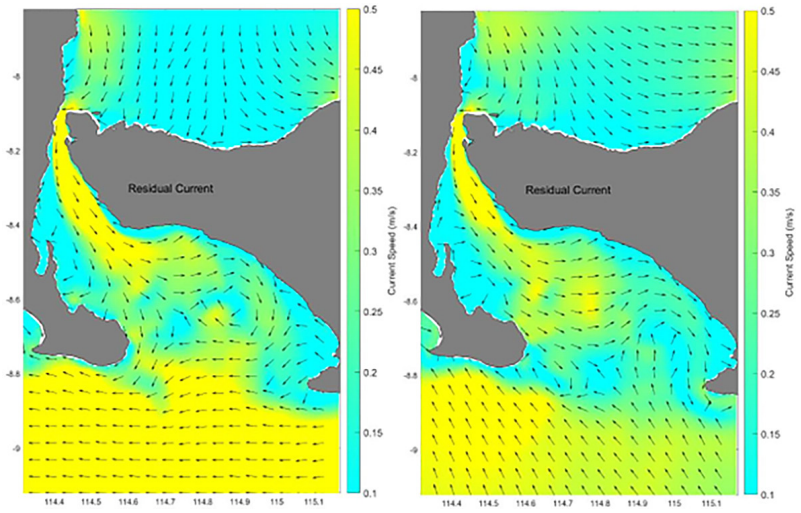

Figure 8. Surface current movement patterns during the southeast monsoon (left) and northwest monsoon (right)

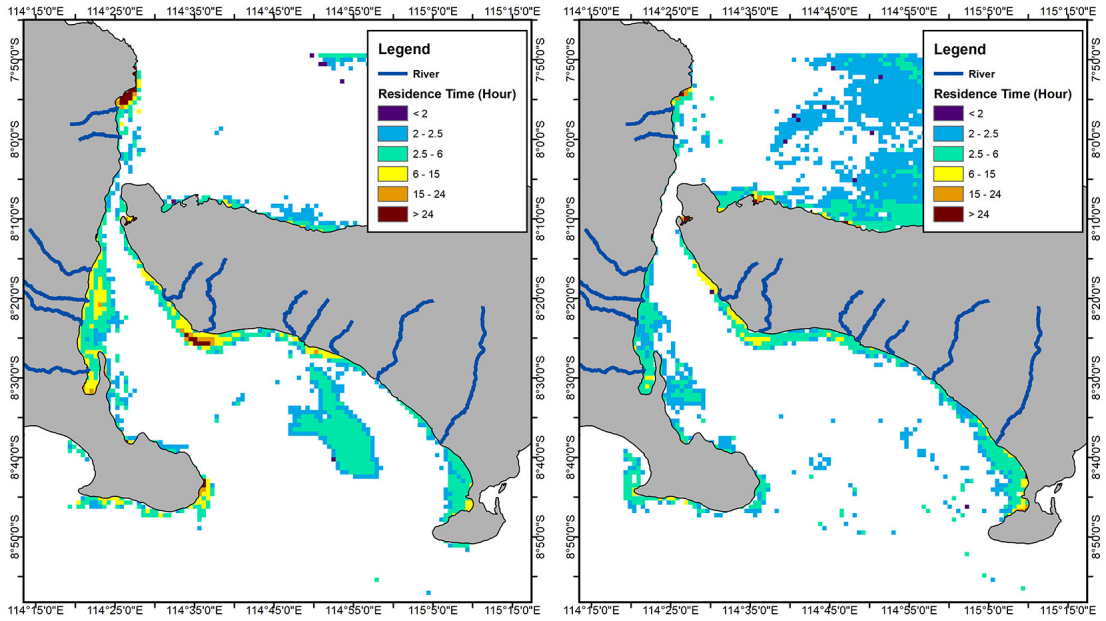

Figure 9. Surface Residence time of plastic during the southeast monsoon (left) and northwest monsoon (right)

The spatial distribution of plastic accumulation derived from Scenario 2, which simulates river source based plastic transport, shows patterns that are broadly consistent with the residence time distribution (Figure 10). During the southeast monsoon, relatively higher plastic density is identified along the eastern coast of Java and within several shallow water areas on the western side of the Bali Strait. Statistically, surface plastic density ranges from 11 to 8.223 pcs km^{-2}, with a mean value of 98.3 pcs km^{-2}. When extreme values are excluded using a trimmed mean approach, the average density decreases to 58 pcs km^{-2}, indicating that the overall distribution is strongly right skewed and dominated by low to moderate density classes, while very high densities occur only locally. In contrast, during the northwest monsoon, zones of higher plastic density shift toward the western coast of Bali Island, particularly along the southern coastline. Statistically, surface plastic density ranges from 11 to 12,387 pcs km^{-2}, with a mean value of 275.3 pcs km^{-2}. When extreme values are excluded using a trimmed mean approach, the average density decreases to 94 pcs km^{-2}, indicating that although the spatial extent of plastic distribution during the northwest monsoon is narrower than during the southeast

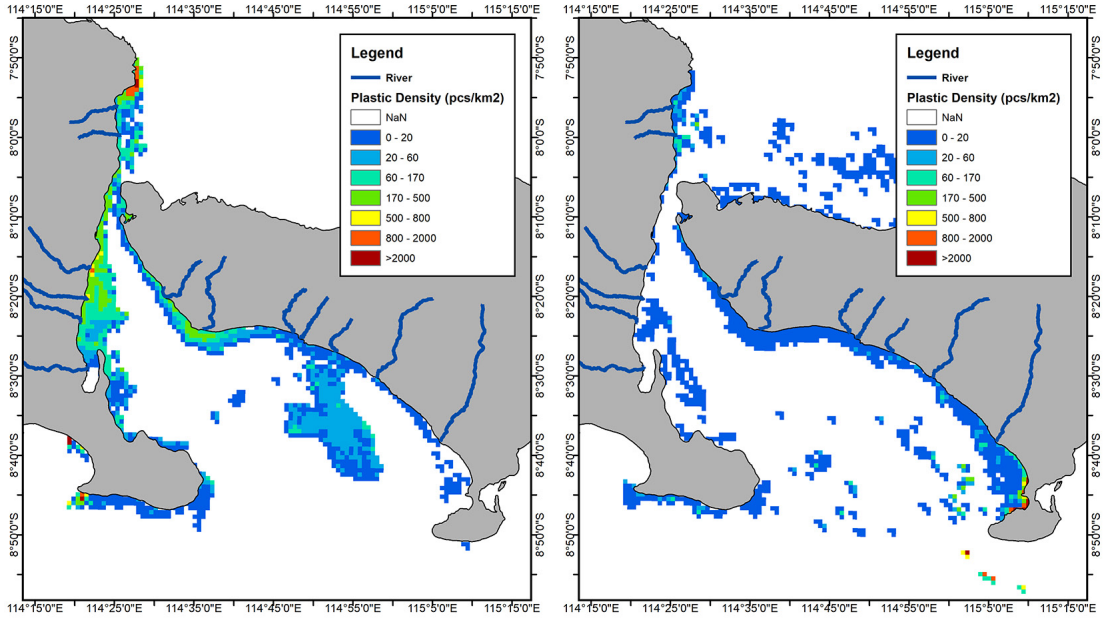

Figure 10. Plastic density during the southeast monsoon (left) and northwest monsoon (right)

monsoon, plastic density is higher and more concentrated along the coast of Badung Regency. Overall, low plastic density values dominate the open waters of the Bali Strait during both seasons, while moderate to high plastic densities are concentrated in nearshore and semi-enclosed areas, highlighting the strong control of seasonal surface circulation on the magnitude and spatial distribution of potential plastic accumulation. These results indicate that seasonal variations in surface circulation strongly control both the magnitude and spatial concentration of surface plastic density and consequently govern the location of potential plastic accumulation zones in the Bali Strait.

Pollution load index distribution across benthic habitats

The PLI values for benthic habitats in the Bali Strait exhibit pronounced spatial and seasonal variability in plastic pollution levels. These PLI values were derived through a spatial overlay analysis that intersected high-retention residence time zones (Figure 9), surface plastic density fields (Figure 10), and benthic ecosystem polygons (Figure 1), whereby surface plastic density values within high retention zones were extracted and spatially aggregated for each benthic habitat. A summary of PLI values and their corresponding classifications for each benthic habitat location is presented in Figure 11.

During the Northwest Monsoon, nearly all locations fall within the Minor category, with relatively low PLI values ranging from 1.91 to 7.53. All sites along the East Java coast, as well as Gilimanuk (Bali), are classified as Minor. The only location deviating from this general pattern is the coast of Badung Regency (Bali), which records a very high PLI value of 41.97 and is classified as Extreme Danger (Figure 11).

In contrast, the Southeast Monsoon is characterized by an overall increase in plastic pollution levels at several locations, particularly along the East Java coast. Alas Purwo and Bama exhibit the highest PLI values, reaching 61.04 and 38.89, respectively, both of which fall within the Extreme Danger category. Other locations, including Teluk Biru, Payaman, Muntjar, and Gilimanuk, are classified as High, with PLI values ranging from 10.03 to 14.40. Meanwhile, Bantenan and Wangsaredja consistently remain within the Minor category during both seasons. During the Southeast Monsoon, the coast of Badung Regency records a PLI value of 0 and is classified as Minor, indicating no detectable plastic accumulation during this period (Figure 11).

Overall, the spatial distribution of PLI categories shown in Figure 11 highlights a clear seasonal contrast: the Northwest Monsoon is characterized by localized plastic accumulation along the coast of Badung Regency, whereas the Southeast Monsoon exhibits more pronounced plastic pollution along the East Java coastline.

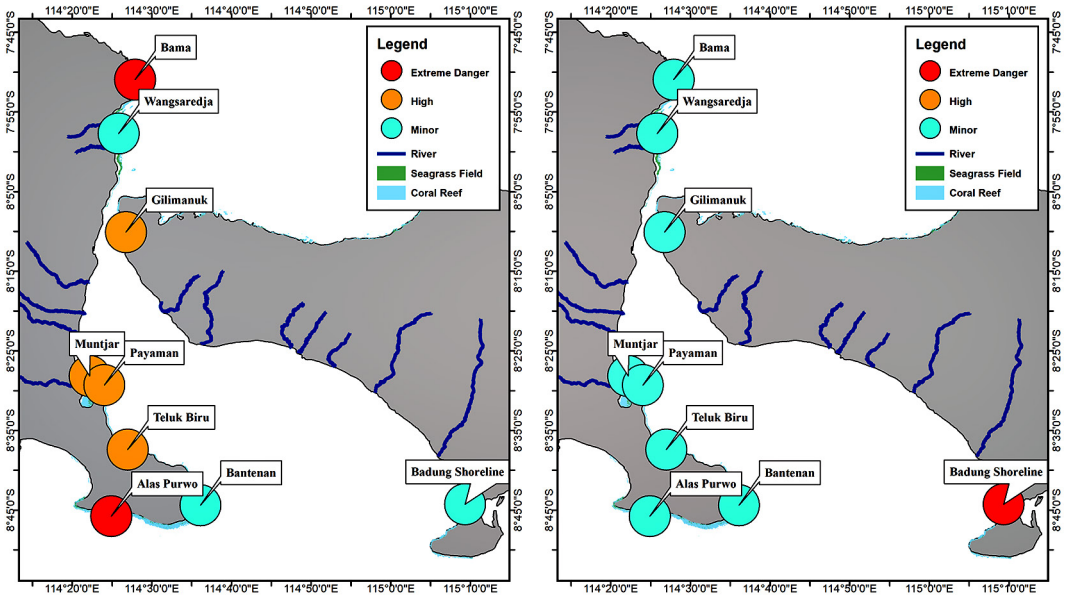

Figure 11. Spatial distribution of plastic PLI categories in the Bali Strait during Southeast Monsoon (left) and Northwest Monsoon (right)

DISCUSSIONS

Seasonal variability of plastic pollution levels based on PLI

The PLI results indicate that plastic pollution levels in benthic ecosystems of the Bali Strait are strongly influenced by the interaction between monsoon driven current dynamics and coastal morphological characteristics. Geographically, the Bali Strait is flanked by the East Java coast to the west and the Bali coast to the east, so changes in monsoon current direction directly affect plastic transport pathways and accumulation locations in both regions (Adibhusana et al., 2023; Maharta et al., 2021). This mechanism is also related to variations in residence time, which determine how long plastic particles are retained in coastal waters before being deposited on the seafloor (Brauwere et al., 2011; Delhez et al., 2014).

During the Northwest Monsoon, dominant surface currents move toward the Bali coast, transporting plastics from rivers discharging along the East Java coast, so that most locations along the East Java coastline remain within the low pollution category (Minor). This condition indicates that plastics entering coastal waters are relatively quickly transported out of the area, resulting in short residence times and low sinking potential. In contrast, the coast of Badung Regency exhibits the highest PLI values, reaching the Extreme Danger category. This pattern is influenced by the concave shoreline, which functions as a natural retention zone and increases the residence time of plastic particles, thereby enhancing the likelihood of sinking and accumulation on the seafloor despite the generally dispersive conditions of the Northwest Monsoon (Maharta et al., 2021). Coral reef ecosystems along the coast of Kuta Beach (Bali) have been shown to receive plastic debris contamination during the Northwest Monsoon (Husrin et al., 2017).

During the Southeast Monsoon, ocean currents reverse direction, causing plastic transport to shift toward the East Java coast. This shift results in a significant increase in PLI values in the Alas Purwo and Bama areas, reaching the Extreme Danger category, as well as increases to the High category in Teluk Biru, Payaman, and Muntjar in East Java and Gilimanuk Bay in Bali. This increase indicates that during the Southeast Monsoon, plastic residence time along the East Java coast and western Bali becomes longer, thereby increasing the likelihood of plastic sinking to the seafloor (Delhez et al., 2014). In contrast, the coast of Badung Regency (Bali) experiences a decrease in PLI to the Minor category, indicating a reduced role of this area as a retention zone when the current direction reverses.

The Gilimanuk area exhibits unique transitional characteristics, as its proximity to the East Java coast makes it sensitive to seasonal changes in current direction. Low PLI values during the

Northwest Monsoon and an increase to the High category during the Southeast Monsoon indicate that Gilimanuk lies along a main plastic transport pathway, with high residence time variability. These results are supported by observations showing that the Gilimanuk area, located near West Bali National Park, also experiences plastic debris pollution along its coastal beaches (Hendrawan et al., 2023). Overall, the PLI patterns confirm that plastic pollution levels in benthic ecosystems of the Bali Strait are dynamic and strongly influenced by monsoon driven circulation mechanisms and coastal morphology.

Implications of benthic plastic pollution levels for ecosystem risk and coastal management

The spatial and seasonal variability of PLI values has important implications for ecological risks in benthic ecosystems of the Bali Strait. Habitats such as coral reefs and seagrass meadows located within zones characterized by high to Extreme Danger PLI levels are likely to experience greater environmental stress, through direct physical interactions with plastics, alterations in sediment quality, and exposure to contaminants associated with plastic debris. This finding is consistent with global evidence indicating that plastic accumulation on the seafloor can exacerbate benthic habitat degradation, particularly in coastal waters with complex circulation dynamics (Kane et al., 2019; UNEP, 2021).

From a coastal management perspective, these results emphasize the importance of a seasonally adaptive approach in the assessment and mitigation of plastic pollution. The shift in high-risk locations between the Northwest and Southeast Monsoon seasons indicates that marine debris monitoring and mitigation strategies cannot be static, but instead must be adjusted in accordance with regional monsoon driven dynamics. This perspective aligns with adaptive management recommendations implemented in several coastal regions of Southeast Asia and other semi-enclosed seas, where seasonal variability plays a critical role in pollution control planning (Lau et al., 2020; Lebreton et al., 2018).

When compared with other tropical coastal regions, the level of benthic plastic pollution in the Bali Strait falls within a range comparable to that reported for coastal ecosystems in the South China Sea. Zheng et al. (2023) demonstrated that PLI values in mangrove, seagrass, and coral reef sediments range from minor to hazardous categories, with strong spatial variability linked to anthropogenic pressure and local hydrodynamic characteristics. The similarity in PLI ranges indicates that a PLI-based approach is effective for assessing benthic plastic pollution levels in tropical coastal ecosystems. The role of seasonal dynamics as a key driver of pollution risk distribution is further supported by studies in other monsoon influenced regions. Gao et al. (2025) reported pronounced contrasts in PLI values between the western and eastern coasts of Peninsular Malaysia, explicitly associated with seasonal variations in winds and surface currents. These findings are consistent with the pattern observed in the Bali Strait, where monsoon driven changes in circulation shift retention zones and plastic accumulation hotspots between seasons, thereby modulating benthic pollution levels both spatially and temporally. Additional support for the influence of monsoon processes is provided by studies from the Indian coast. Kalangutkar et al. (2025) reported PLI values indicating contaminated conditions in the Terekhol and Sal estuaries during the monsoon season, which were linked to increased river discharge and coastal activities as primary sources of microplastics. Similarly, Raju et al. (2023) showed that PLI values and polymer hazard levels along the eastern coast of India increased significantly during the northeast monsoon, when wind and current patterns were conducive to microplastic accumulation. Although these studies focus on beach and estuarine environments, the shared monsoon controlled physical mechanisms reinforce the interpretation that the seasonal variability of benthic PLI observed in the Bali Strait is part of a broader regional pattern characteristic of monsoon dominated tropical marine systems.

Taken together, the findings from the Bali Strait and their comparison with other monsoon influenced coastal systems indicate that benthic plastic pollution is governed by a consistent set of physical and geographic controls, in which seasonal circulation, coastal orientation, and shoreline morphology jointly regulate plastic retention and accumulation on the seafloor. The spatial–seasonal PLI patterns observed in the Bali Strait align with evidence from the South China Sea, Peninsular Malaysia, and the Indian coast, suggesting that monsoon driven variability represents a fundamental mechanism shaping

benthic plastic pollution risk across tropical regions. In this context, integrating PLI with an understanding of monsoon controlled hydrodynamics provides a robust and transferable framework for assessing benthic plastic pollution, enabling the identification of seasonally vulnerable habitats and supporting adaptive, region-specific management strategies in coastal and strait environments characterized by strong seasonal circulation.

CONCLUSIONS

This study demonstrates that plastic pollution levels in benthic ecosystems of the Bali Strait vary both spatially and seasonally, as reflected by differences in PLI values across locations and monsoon periods. The PLI evaluation indicates that several coastal areas experience high to extreme pollution levels during specific seasons, driven by the interaction between seasonal current dynamics, coastal geographic position, and shoreline morphological characteristics.

Seasonally, the highest levels of benthic plastic pollution during the Southeast Monsoon are identified along the western side of the Bali Strait, particularly in the Alas Purwo and Bama areas. In contrast, during the Northwest Monsoon, pollution risk shifts toward the western and southern coasts of Bali, especially along Kuta Beach. Integrating the PLI with information on hydrodynamic processes enables a more contextual and operational assessment of benthic plastic pollution, providing a robust basis for identifying high-risk habitats and supporting the prioritization of monitoring and management strategies in ecologically valuable and anthropogenically pressured coastal regions.

Acknowledgement

The author acknowledges financial support from the Natural Environment Research Council (NERC) (grant number NE/V006428/1) through the project "PISCES: A Systems Analysis Approach to Reduce Plastic Waste in Indonesian Societies", which supported the author's academic study and research contributing to this manuscript.

REFERENCES

1. Adibhusana, M. N., Hendrawan, I. G., Ryu, Y. (2023). Numerical study on tide and tidal current along Bali Strait, Indonesia using finite volume coastal ocean model (FVCOM). *Korea Society of Coastal Disaster Prevention, 10*(1), 35–40. https://doi.org/10.20481/kscdp.2023.10.1.35
2. Auta, H. S., Emenike, C. U., Fauziah, S. H. (2017). Distribution and importance of microplastics in the marine environment: A review of the sources, fate, effects, and potential solutions. *Environment International, 102*, 165–176. https://doi.org/10.1016/j.envint.2017.02.013
3. Bergmann, M., Lutz, B., Tekman, M. B., Gutow, L. (2017). Citizen scientists reveal : Marine litter pollutes Arctic beaches and a ff ects wild life. *Marine Pollution Bulletin, 125*(1–2), 535–540. https://doi.org/10.1016/j.marpolbul.2017.09.055
4. Boakes, Z., Hall, A. E., Elvan, E., Jones, G. C. A., Ngurah, I. G., Suryaputra, A., Putu, L., Prasetijo, R., & Stafford, R. (2022). Coral reef conservation in Bali in light of international best practice, a literature review. *Journal for Nature Conservation, 67*(April), 126190. https://doi.org/10.1016/j.jnc.2022.126190
5. Brauwere, A. De, Brye, B. De, Blaise, S., Deleersnijder, E. (2011). Residence time, exposure time and connectivity in the Scheldt Estuary. *Journal of Marine Systems, 84*(3–4), 85–95. https://doi.org/10.1016/j.jmarsys.2010.10.001
6. Bucknall, D. G. (2020). *Plastics as a materials system in a circular economy: Plastics in the Circular Economy.* In Philosophical Transactions of the Royal Society A: Mathematical, Physical and Engineering Sciences 378, 2176. https://doi.org/10.1098/rsta.2019.0268
7. Chai, T., Draxler, R. R. (2014). Root mean square error (RMSE) or mean absolute error (MAE)? – Arguments against avoiding RMSE in the literature. *Geoscientific Model Development, 7*(3), 1247–1250. https://doi.org/10.5194/gmd-7-1247-2014
8. Chen, C., Beardsley, R. C., Cowles, G. (2006). An unstructured-grid, finite-volume coastal ocean model (FVCOM) system. *Oceanography, 19*(SPL.ISS. 1), 78–89. https://doi.org/10.5670/oceanog.2006.92
9. Cordova, M. R., Iskandar, M. R., Muhtadi, A., Nurhasanah, Saville, R., Riani, E. (2022). Spatio-temporal variation and seasonal dynamics of stranded beach anthropogenic debris on Indonesian beach from the results of nationwide monitoring. *Marine Pollution Bulletin, 182*(April), 114035. https://doi.org/10.1016/j.marpolbul.2022.114035
10. Cózar, A., Sanz-Martín, M., Martí, E., González-Gordillo, J. I., Ubeda, B., Á.gálvez, J., Irigoien, X., Duarte, C. M. (2015). Plastic accumulation in the mediterranean sea. *PLoS ONE, 10*(4), 1–12. https://doi.org/10.1371/journal.pone.0121762

11. Critchell, K., Grech, A., Schlaefer, J., Andutta, F. P., Lambrechts, J., Wolanski, E., Hamann, M. (2015). Modelling the fate of marine debris along a complex shoreline: Lessons from the Great Barrier Reef. *Estuarine, Coastal and Shelf Science, 167*, 414–426. https://doi.org/10.1016/j.ecss.2015.10.018
12. Critchell, K., Lambrechts, J. (2016). Estuarine, Coastal and Shelf Science Modelling accumulation of marine plastics in the coastal zone ; what are the dominant physical processes ? *Estuarine, Coastal and Shelf Science, 171*, 111–122. https://doi.org/10.1016/j.ecss.2016.01.036
13. Delhez, É. J. M., Brye, B. De, Brauwere, A. De, Deleersnijder, É. (2014). Residence time vs in fluence time. *Journal of Marine Systems 132*, 185–195. https://doi.org/10.1016/j.jmarsys.2013.12.005
14. Derraik, J. G.. (2002). The pollution of the marine environment by plastic debris: a review. *Marine Pollution Bulletin, 44*(9), 842–852. https://doi.org/10.1016/S0025-326X(02)00220-5
15. Gao, P., Matheus, D., Hu, W., Chen, W., Fadhullah, W., John, A. (2025). Regional studies in marine science marine microplastic pollution in Peninsular Malaysia: A meta-analysis. *Regional Studies in Marine Science, 86*(May), 104228. https://doi.org/10.1016/j.rsma.2025.104228
16. Harding, S. (2016). *Marine Debris: Understanding, Preventing and Mitigating the Significant Adverse Impacts on Marine and Coastal Biodiversity.* Technical Series No.83. Secretariat of the Convention on Biological Diversity. In CBD Technical Series 1(83). Secretariat of the Convention on Biological Diversity.
17. Hendrawan, I. G., Pamungkas, P. B. P., Adibhusana, M. N., Maharta, I. P. R. F., Saraswati, N. L. G. R. A., Wilcox, C., Hardesty, B. D. (2023). Characteristics and distribution of stranded plastic pollution in Bali conservation areas. *Marine Pollution Bulletin, 197*(November), 115770. https://doi.org/10.1016/j.marpolbul.2023.115770
18. Husrin, S., Wisha, U. J., Prasetyo, R., Putra, A., Attamimi, A. (2017). Characteristics of marine litters in the west coast of Bali. *Jurnal Segara, 13*(2), 129–140. https://doi.org/10.15578/segara.v13i2.6449
19. Intyas, C. A., Koestiono, D., Tjahjono, A., Suhartini, S. (2025). Assessing the sustainable supply chain management performance of ornamental coral in the Bali strait using the RAPFish method. https://doi.org/10.5755/j01.erem.81.3.39725
20. Jambeck, J. R., Geyer, R., Wilcox, C., Siegler, T. R., Perryman, M., Andrady, A., Narayan, R., Law, K. L. (2015). Plastic waste inputs from land into the ocean. *Science, 347*(6223), 768–771. https://doi.org/10.1126/science.1260352
21. Kalangutkar, N., Mhapsekar, S., Rajagopal, P. (2025). Comparative assessment of microplastic pollution in Terekhol and Sal estuaries, Goa, India. *Environmental Earth Sciences, 84*(1), 48. https://doi.org/10.1007/s12665-024-12042-x
22. Kane, I. A., Clare, M. A., Hodgson, D. M., Kane, I. A. (2019). Dispersion, accumulation, and the ultimate fate of microplastics in deep-marine environments : A review and future directions. 7(April). https://doi.org/10.3389/feart.2019.00080
23. Kooi, M., Nes, E. H. Van, Koelmans, A. A. (2017). Ups and downs in the ocean: Effects of biofouling on vertical transport of microplastics. *Environmental Science & Technology.* https://doi.org/10.1021/acs.est.6b04702
24. Lambert, C., Authier, M., Dorémus, G., Laran, S., Panigada, S., Spitz, J., Van Canneyt, O., Ridoux, V. (2020). Setting the scene for Mediterranean litterscape management: The first basin-scale quantification and mapping of floating marine debris. *Environmental Pollution, 263.* https://doi.org/10.1016/j.envpol.2020.114430
25. Lau, W. W. Y., Shiran, Y., Bailey, R. M., Cook, E., Stuchtey, M. R., Koskella, J., Velis, C. A., Godfrey, L., Boucher, J., Murphy, M. B., Thompson, R. C., Jankowska, E., Castillo, A. C., Pilditch, T. D., Dixon, B., Koerselman, L., Kosior, E., Favoino, E., Gutberlet, J., …, Palardy, J. E. (2020). Evaluating scenarios toward zero plastic pollution. *Science, 369*(6509). https://doi.org/10.1126/SCIENCE.ABA9475
26. Lebreton, L., Slat, B., Ferrari, F., Sainte-Rose, B., Aitken, J., Marthouse, R., Hajbane, S., Cunsolo, S., Schwarz, A., Levivier, A., Noble, K., Debeljak, P., Maral, H., Schoeneich-Argent, R., Brambini, R., Reisser, J. (2018). Evidence that the great pacific garbage patch is rapidly accumulating plastic. *Scientific Reports, 8*(1), 1–15. https://doi.org/10.1038/s41598-018-22939-w
27. Liubartseva, S., Coppini, G., Lecci, R., Clementi, E. (2018). Tracking plastics in the mediterranean: 2D Lagrangian model. *Marine Pollution Bulletin, 129*(1), 151–162. https://doi.org/10.1016/j.marpolbul.2018.02.019
28. Maharta, I. P. R. F., Radjawane, I. M., Hendrawan, I. G. (2020). Study of Debris Movement in South and West Coast of Sumatra and Java and Its Impact on Bali Strait during Western Monsoon. *IOP Conference Series: Earth and Environmental Science, 618*(1). https://doi.org/10.1088/1755-1315/618/1/012009
29. Maharta, I. P. R. F., Radjawane, I. M., Suprijo, T., Park, H., Hendrawan, I. G. (2021). Identification of Marine Debris Sources in Kuta Beach, Bali, Indonesia. *Journal of Coastal Research, 114*(sp1), 594–598. https://doi.org/10.2112/JCR-SI114-120.1
30. Maximenko, N., Hafner, J., Niiler, P. (2012). Pathways of marine debris derived from trajectories of Lagrangian drifters. *Marine Pollution Bulletin, 65*(1–3), 51–62. https://doi.org/10.1016/j.

marpolbul.2011.04.016

31. Napper, I. E., Baroth, A., Barrett, A. C., Bhola, S., Chowdhury, G. W., Davies, B. F. R., Duncan, E. M., Kumar, S., Nelms, S. E., Hasan, N., Nishat, B., Maddalene, T., Thompson, R. C., Koldewey, H. (2021). The abundance and characteristics of microplastics in surface water in the transboundary Ganges River *. *Environmental Pollution, 274*, 116348. https://doi.org/10.1016/j.envpol.2020.116348
32. Clayer, F., Norling, M. D., Fürst, K., Hurley, R., Creencia, G. B. A., Msojica, D. Z. P., Dizon, J. C. R., Lin, Y., Nizzetto, L., Sedigo, N. A., Olsen, M., Veiteberg Braten, H. F. (2024). Modelling plastic fluxes with INCA-macroplastics in the Imus catchment: impacts of long-term accumulation and extreme events. *Environmental Research Letters, 19*(1), 015001. https://doi.org/10.1088/1748-9326/ad163f
33. Patterson, J., Jeyasanta, K. I., Laju, R. L., Booth, A. M., Sathish, N., Edward, J. K. P. (2022a). Microplastic in the coral reef environments of the Gulf of Mannar, India - Characteristics, distributions, sources and ecological risks. *Environmental Pollution, 298*(January), 118848. https://doi.org/10.1016/j.envpol.2022.118848
34. Patterson, J., Jeyasanta, K. I., Laju, R. L., Booth, A. M., Sathish, N., Edward, J. K. P. (2022b). Microplastic in the coral reef environments of the Gulf of Mannar, India - Characteristics, distributions, sources and ecological risks *. *Environmental Pollution, 298*(January), 118848. https://doi.org/10.1016/j.envpol.2022.118848
35. Paul, A., Machado, M., Thomas, A., Turra, A. (2017). Transboundary movement of marine litter in an estuarine gradient : Evaluating sources and sinks using hydrodynamic modelling and ground truthing estimates. *Marine Pollution Bulletin, 119*(1), 48–63. https://doi.org/10.1016/j.marpolbul.2017.03.034
36. Pearson, K. (1895). X. Contributions to the mathematical theory of evolution.—II. Skew variation in homogeneous material. *Philosophical Transactions of the Royal Society of London, Series A: Containing Papers of a Mathematical or Physical Character, 186*, 343–414. https://doi.org/10.1098/rsta.1895.0010
37. Politikos, D. V., Tsiaras, K., Papatheodorou, G., Anastasopoulou, A. (2020). Modeling of floating marine litter originated from the Eastern Ionian Sea: Transport, residence time and connectivity. *Marine Pollution Bulletin, 150*(October 2019), 110727. https://doi.org/10.1016/j.marpolbul.2019.110727
38. Praved, P. H., Neethu, K. V, Nandan, S. B., Krishna, N. G. A., Aneesh, B. P., Sankar, N. D., Antony, H., Aravind, E. H. (2025). Multidimensional risk assessment of marine litter pollution in the ecologically fragile coral atolls of India. *Journal of Environmental Management, 376*(July 2024), 124578. https://doi.org/10.1016/j.jenvman.2025.124578
39. Raju, M. P., Veerasingam, S., Suneel, V., Saha, M., Rathore, C., Naik, A., Suneetha, P., Ramakrishna, S. S. V. S. (2023). Seasonal variation and spatial distribution of microplastic pellets and their associated contaminants along the central east coast of India. *Environmental Science and Pollution Research, 30*(26), 68489–68503. https://doi.org/10.1007/s11356-023-27100-3
40. Rosas, E., Martins, F., Tosic, M., Janeiro, J., Mendonça, F., Mills, L. (2022). Pathways and Hot Spots of Floating and Submerged Microplastics in Atlantic Iberian Marine Waters: A Modelling Approach. *Journal of Marine Science and Engineering, 10*(11). https://doi.org/10.3390/jmse10111640
41. Rothäusler, E., Jormalainen, V., Gutow, L., Thiel, M. (2019). Low abundance of floating marine debris in the northern Baltic Sea. *Marine Pollution Bulletin, 149*(April), 110522. https://doi.org/10.1016/j.marpolbul.2019.110522
42. Suteja, Y., Atmadipoera, A. S., Riani, E., Nurjaya, I. W., Nugroho, D., Purwiyanto, A. I. S. (2021). Stranded marine debris on the touristic beaches in the south of Bali Island, Indonesia: The spatiotemporal abundance and characteristic. *Marine Pollution Bulletin, 173*(PA), 113026. https://doi.org/10.1016/j.marpolbul.2021.113026
43. Thushari, G. G. N., Senevirathna, J. D. M. (2020). Heliyon Plastic pollution in the marine environment. *HLY, 6*(8), e04709. https://doi.org/10.1016/j.heliyon.2020.e04709
44. Tomlinson, D. L., Wilson, J. G., Harris, C. R., Jeffrey, D. W. (1980). Problems in the assessment of heavy-metal levels in estuaries and the formation of a pollution index. *Helgoländer Meeresuntersuchungen, 33*(1), 566–575. https://doi.org/10.1007/BF02414780
45. Uncles, R., Clark, J., Bedington, M., Torres, R. (2020). On sediment dispersal in the Whitsand Bay marine conservation zone: Neighbour to a closed dredge-spoil disposal site. In *Marine protected areas* 599–629. Elsevier. https://doi.org/10.1016/B978-0-08-102698-4.00031-9
46. UNEP (United Nations Environment Programme). (2021). From pollution to solution: a global assessment of marine litter and plastic pollution. In *New Scientist 237*(3169). https://www.unep.org/resources/pollution-solution-global-assessment-marine-litter-and-plastic-pollution.
47. van Sebille, E., Wilcox, C., Lebreton, L., Maximenko, N., Hardesty, B. D., van Franeker, J. A., Eriksen, M., Siegel, D., Galgani, F., Law, K. L. (2015). A global inventory of small floating plastic debris. *Environmental Research Letters, 10*(12), 124006. https://doi.org/10.1088/1748-9326/10/12/124006

48. Wang, X., Liu, K., Zhu, L., Li, C., Song, Z., Li, D. (2021). Efficient transport of atmospheric microplastics onto the continent via the East Asian summer monsoon. *Journal of Hazardous Materials, 414*(November 2020), 125477. https://doi.org/10.1016/j.jhazmat.2021.125477
49. Willmott, C., Matsuura, K. (2005). Advantages of the mean absolute error (MAE) over the root mean square error (RMSE) in assessing average model performance. *Climate Research, 30*, 79–82. https://doi.org/10.3354/cr030079
50. Willmott, C. J., Robeson, S. M., Matsuura, K. (2012). A refined index of model performance. *International Journal of Climatology, 32*(13), 2088–2094. https://doi.org/10.1002/joc.2419
51. Wu, Y., Law, B., Ding, F., O'Flaherty-Sproul, M. (2022). Modeling the effect of cage drag on particle residence time within fish farms in the Bay of Fundy. *Aquaculture Environment Interactions, 14*, 163–179. https://doi.org/10.3354/aei00434
52. Yin, Y., Mohd, N., Weston, K., Talib, M., Suratman, S., Uzair, M., Mayes, A. G. (2023). Science of the total environment atmospheric microplastic transport and deposition to urban and pristine tropical locations in Southeast Asia. *Science of the Total Environment, 902*(August), 166153. https://doi.org/10.1016/j.scitotenv.2023.166153
53. Zheng, X., Sun, R., Dai, Z., He, L., Li, C. (2023). Science of the total environment distribution and risk assessment of microplastics in typical ecosystems in the South China Sea. *Science of the Total Environment, 883*(April), 163678. https://doi.org/10.1016/j.scitotenv.2023.163678
54. Zhou, X., Zhu, G., Hu, S. (2020). Influence of tides on mass transport in the Bransfield Strait and the adjacent areas, Antarctic. *Polar Science, 23*(December 2019), 100506. https://doi.org/10.1016/j.polar.2020.100506